Appl. Phys. B. 60, 199–204 (1995)

Applied Physics B Lasers and Optics

Topological phase shift in a cold-atom interferometer

J.H. Müller, D. Bettermann, V. Rieger, K. Sengstock, U. Sterr, W. Ertmer

Institut für Angewandte Physik, Wegelerstrasse, 8, D-53115 Bonn, Germany
(Fax: + 49-228/73-3474, E-mail: JHM @ serv.iap.uni-bonn.de)

Received: 20 September 1994/Accepted: 2 November 1994

Abstract. Matter-wave interferences in a four-pulse version of a Ramsey-Bordé atom interferometer have been utilized to study phase shifts. A topological phase shift analogous to the scalar Aharonov-Bohm effect proposed for charged-particle interferences in the presence of a pulsed electrostatic potential has been investigated. The time-dependent potential has been generated by the interaction of a laser field with an induced atomic dipole without spatial variation along the interferometer arms. The atom interferometer has been run with laser-cooled magnesium atoms stored in a magneto-optical trap.

PACS: 03.65.Bz; 03.75.Be; 32.80.Pj

The recent successful realizations of atom interferometers [1–6] has intensified the interest to perform fundamental experiments with this new kind of matter-wave interferometers [3, 5, 7–12]. Compared to electrons, atoms are only weakly influenced by electric fields so that technical problems with stray fields often encountered in the earlier developed electron interferometers [13] are of no relevance here. With regard to neutron interferometry [14, 15], the sources for interfering atoms can be built much more compact even allowing portable devices. The complex internal structure of atoms and the easy access to the inner degrees of freedom opens the way to qualitatively new kinds of experiments, e.g., to explore the interaction of atoms with quantized radiation fields with matter-wave interferometric techniques [16, 17].

The pulsed version of Ramsey-Bordé interferometry [12, 18] is particularly suited to investigate the effect of a time-dependent scalar potential on the interference signal. The basic idea of pulsed Ramsey-Bordé interferometry is visualized conveniently with a recoil diagram [19, 20]. Consider a two-level atom with upper (lower) level designated $|e>$ ($|g>$) interacting coherently with four laser pulses resonant with the transition between the two levels (Fig. 1). The first laser pulse splits the incoming ground-state atomic wave packet into two parts differing in momentum by one photon recoil $\hbar k$ and propagating in different internal states. The next two pulses perform further splitting and redirecting of the wave-packet trajectories, while the fourth pulse acts as the output-port beam splitter of the interferometer. Closed paths for the wave packets are achieved with two counterpropagating pairs of collinear laser pulses separated in time by equal intervals T. These closed paths fulfill the conditions for white-light interference, i.e., the output phase of the signal is independent of the initial momentum of the wave packet. Furthermore, the spatial coherence length of the wave packet does not restrict the interference visibility as a function of laser frequency in contrast to stationary Ramsey-Bordé interferometry with atomic *beams*. The output ports of the interferometer differ in the internal state of the atom, allowing to read out the interferometric signal simply by monitoring the population of the internal states.

Tracing the phase evolution along the closed paths leads to the known dependence of the phase Φ_{out} of the interference signal on the parameters of the laser pulses [21]:

$$\Phi_{out} = 2(\Delta \pm \delta)\, T + \Phi_L + \Phi_{add}. \quad (1)$$

Here, Δ denotes the detuning between the atomic resonance and the laser frequency, T denotes the delay between copropagating pulses, δ denotes the recoil shift $\hbar k^2/2m$ and the Φ_L depends on the phase differences between the laser pulses. The additional phases Φ_{add} accounts for the influence of external perturbations like those discussed in the following section. The interference signal consists of two fringe systems separated in frequency space by the recoil splitting 2δ. The phase of the interference signal can be scanned either by varying the phase difference of the laser pulses or by scanning the detuning Δ [22]. This explicit dependence of the interference signal on the laser

Dedicated to H. Walther on the occasion of his 60th birthday

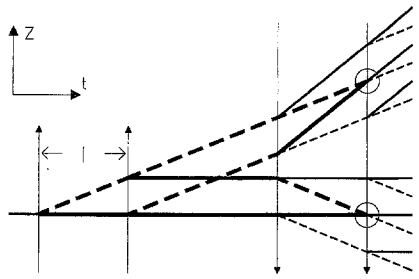

Fig. 1. Recoil diagram of the four-pulse Ramsey-Bordé interferometer. The splitting of the wave-packet trajectories due to the transfer-photon momenta is shown vs time. The partial wave packets propagate in the ground (excited) state along the *solid (broken) lines*. The closed trapezoids (*thick lines*) correspond to the two recoil components of the interference signal

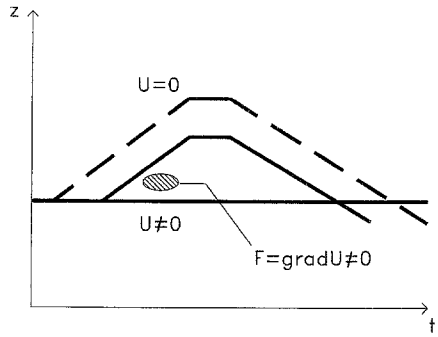

Fig. 2. Interferometric paths in space-time encircling a region of non-vanishing gradient of a scalar potential. The amount of enclosed generalized flux does not depend on variations of the path outside the *hatched region*

detuning is utilized in high-resolution spectroscopy [23, 24].

In the following section, the influence of additional potentials on the interference signal is discussed and the analogy between an experiment proposed originally for an electron interferometer by Aharonov and Bohm in 1959 [25] and the experiment performed in the course of this work is established. The special case of a light-shift potential to the pulsed Ramsey-Bordé interferometer is introduced in Sect 2, and experimental signatures of a resulting topological phase shift are discussed. Section 3 is devoted to the description of the experimental setup and the obtained results. The paper closes with a brief outlook to future developments.

1 Topological phase shifts due to enclosed fluxes

For a matter-wave interferometer we consider additional potentials $\mathbf{V}(\mathbf{r})$ and $U(\mathbf{r}, t)$ which enter the Hamiltonian as a modification of the canonical momentum or as a scalar potential, respectively:

$$\hat{\mathscr{H}} = \hat{\mathscr{H}}_i + [\hat{\mathbf{p}} - \mathbf{V}(\hat{\mathbf{r}})]^2/2m + U(\hat{\mathbf{r}}, t) \tag{2}$$

Here, $\mathbf{V}$ and U describe, e.g., the electromagnetic interaction of charged particles with external fields or the pseudopotentials occurring in non-inertial systems. The term $\hat{\mathscr{H}}_i$ contains the interaction with the beam-splitting and redirecting devices and determines the quasiclassical trajectory of the interfering wave packets. The phase shift Φ_{add}, due to the additional potentials, can be calculated to first order as the modification of the action integral along the undistributed path Γ:

$$\Phi_{\text{add}} = \frac{1}{\hbar}\int_{\Gamma} V(\mathbf{r})\,\mathrm{d}\mathbf{r} - \mathrm{U}(\mathbf{r},t)\,\mathrm{d}t$$

$$= \frac{1}{\hbar}\int_{\mathrm{O}(\Gamma)} \nabla\times\mathbf{V}(\mathbf{r})\mathrm{d}\boldsymbol{O} - \frac{1}{\hbar}\int_{\mathrm{O}'(\Gamma)} \nabla\mathrm{U}(\mathbf{r},t)\mathrm{d}\mathbf{r}\,\mathrm{d}t. \tag{3}$$

Here, Stoke's theorem has been used to cast the contribution from the vector potential in an integral over the surface $\mathrm{O}(\Gamma)$ enclosed by the path in real space. The second term is written as an integral over the surface $\mathrm{O}'(\Gamma)$ spanned by the path in space-time, introducing the integrand as a generalized flux density [26, 27]. Evaluation of the phase shift for spatially constant fields $\nabla\times\mathbf{V}$ and $\nabla\mathrm{U}$ shows the well-known proportionality between the phase shift and the area enclosed by the undisturbed paths of the interfering wave packet.

Table 1. Classification of several variations of the Aharonov-Bohm effect for interfering particles possessing charge, magnetic, or electric dipole moments

Vector potential	$\mathbf{V}$	Theory	Observed using
Charge q	$-\mathrm{q}\cdot\mathbf{A}$	[25]	$\bar{\mathrm{e}}$ [28]
Magnetic dipole $\boldsymbol{\mu}$	$-(\boldsymbol{\mu}\times\mathbf{E})/c^2$	[29, 30]	n [31], ThF [32]
Electric dipole $\mathbf{d}$	$-(\mathbf{d}\times\mathbf{B})$	[26, 33]	Not observed
Scalar potential	U		
Charge q	$-\mathrm{q}\cdot\Phi$	[25]	Not observed
Magnetic dipole $\boldsymbol{\mu}$	$-\boldsymbol{\mu}\cdot\mathbf{B}$	[34]	n [35, 36], H [37]
Electric dipole $\mathbf{d}$	$-\mathbf{d}\cdot\mathbf{E}$	[26, 33]	Mg [this work]

A special situation arises when the fields vanish along the undisturbed paths, but are different from zero in a region enclosed by the paths. Although all forces and torques vanish along the classical path and hence no classical observable is changed, a detectable phase shift still remains. Because the amount of enclosed flux does not vary with the shape of the paths, the magnitude of the phase shift is independent from the enclosed area (Fig. 2). The phase shift remains even if external boundaries exclude the region of non-zero fields from the allowed regions of the wave function, i.e., interference takes place in multiple connected region. The resulting phase shift caused by the enclosed flux is thus called topological. Phase shifts of this type are well known since the studies of Aharonov and Bohm, who considered the interference of charged particles in the presence of enclosed electromagnetic fluxes [25]. While the proposed effect of an enclosed magnetic flux has been confirmed experimentally soon after the publication of Aharonov and Bohm by Chambers [28], an experimental test of the related scalar effect with charged particles is still lacking.

As suggested by the reasoning at the beginning of this section, the basic idea of topological phase shifts due to enclosed fluxes can be extended to various kinds of potentials. The interaction of particles carrying magnetic or electric-dipole moments with magnetic and electric fields has been considered theoretically and experimentally by different authors (see Table 1). The remainder of this

paper is devoted to an experiment where the interaction of an induced electric-dipole moment with the inducing field leads to the topological phase shift.

2 The pulsed light-shift potential

A convenient choice for an additional scalar potential in an atom interferometer is given by the interaction of a light field nearly resonant with an allowed transition of the atom with the induced oscillating dipole moment. Due to the entanglement of internal and external states in the pulsed Ramsey-Bordé interferometer, the original idea of the Aharonov-Bohm can be transferred without the need of an excluded spatial region, if a state-selective potential is applied. Here, the internal structure of the atom shelves one arm of the interferometer from sensing the potential.

The level scheme of the Mg atoms suggests the use of the spin- forbidden $^1S_0$–$^3P_1$ transition for interferometry, while the strong principal transition in the singlet system $^1S_0$–$^1P_1$ is ideally suited for the generation of a light-shift potential. Laser light detuned from the strong transition by Δ_{uv} shifts the energy of the ground level by

$$\delta E = -\frac{\hbar\Delta_{uv}}{2}[1-\sqrt{1+(\Omega/\Delta_{uv})^2}]. \tag{4}$$

Here, Ω denotes the Rabi frequency, where $\Omega^2 \propto I$ is a measure of the laser intensity I. This energy shift is considered as a scalar potential for the center-of-mass motion of the ground-state part of the atom only, while the excited $^3P_1$-state part is unaffected by the light. In the limit of large detuning $\Delta_{uv} \gg \Omega$, the energy shift can be expanded to:

$$\delta E \approx \frac{\hbar\Omega^2}{4\Delta_{uv}} \tag{5}$$

The values for laser intensity, detuning and their temporal variation have to be chosen in a way ensuring adiabatic evolution of the population in the dressed state evolving from the ground state during the pulse and to minimize spontaneous decay losses due to admixture of the $^1P_1$ state. These requirements are best fulfilled for large detuning values and inverse rise times of the Rabi frequency small compared to the detuning.

The phase shift $\delta\phi$ due to the light-shift pulse of duration T' is calculated to be:

$$\Phi_{\text{add}} = -\frac{1}{\hbar}\int \mathrm{U}(t)\mathrm{d}t = -\frac{1}{\hbar}\int_0^T \frac{\hbar\Omega^2(t)}{4\Delta}\mathrm{d}t. \tag{6}$$

In order to prevent the atoms from sensing a non-vanishing gradient of the potential, the spatial intensity distribution of a laser beam shifting the ground-state energy has to be large compared to the dimensions of the interferometer. The transient acceleration during the switching time of the potential due to the finite propagation velocity c of the potential leads to an additional phase shift, which is smaller than Φ_{add} by a factor v/c. Since the velocity v of the interfering atoms in our experiment is of the order 1 m/s, this additional phase is negligibly small.

An experimental signature for the topological nature of the phase shift can be derived by showing its independence from the shape of the interferometric path in space-time. With pulsed Ramsey-Bordé interferometry, this can be done by varying the delay T between equivalent beam-splitter pulses, while keeping the parameters of the light-shift pulse fixed. A second way of proving the assumption is to monitor the contrast of the interference signal for different values of the phase shift. Any force acting differentially on the wave packets in the arms of the interferometer leads to a decreasing overlap at the output-port beam splitter, hence, to a considerably reduced contrast if the differential shift of the wave packets exceeds the coherence length of the packets. The coherence length is determined by the inverse width of the momentum distribution of the atoms contributing to the interference signal. Since we use cold ^{24}Mg atoms for interferometry with momentum spreads in the range of 1 m/s perpendicularly to the direction of the beam-splitter pulses and about 0.2 m/s in the direction of the beam-splitter pulses, the coherence lengths are about 15 nm and 75 nm, respectively. This has to be compared to Ramsey-Bordé interferometers using thermal atomic beams, where a typical value for the coherence length is 33 pm [9]. Thus, the sensitivity of the contrast to spatial shifts of the packets due to differential forces inside the cold-atom interferometer is rather small.

3 Experimental setup and results

The cold atomic ensemble for interferometry is prepared in a magneto-optical trap (Fig. 3). Mg atoms either from a thermal or a laser-slowed atomic beam are stored in the trap operating on the strong $^1S_0$–$^1P_1$ transition at 285.2 nm. A frequency-double (SHG) dye laser at 570 nm provides the necessary UV radiation. Typical values for the number of trapped atoms are 10^3 captured from a thermal beam and 4×10^5 from the laser-slowed beam. The temperature of the atoms measured with a time-of-flight technique is close to the Doppler limit corresponding to a rms velocity of $\alpha_v = 0.81$ m/s. The diameter d of the cloud of trapped atoms is typically d = 300 μm. The trap fluorescence decays exponentially when the loading is switched from the slowed source to the thermal beam with a time constant typically about $\tau = 0.5$ s. We use the trap dynamics for a signal amplification of the interference signal as discussed in [18] and briefly below.

The light pulses for interferometry on the $^1S_0$–$^3P_1$ transition are delivered by an ultrastable dye-laser spectrometer at 457 nm. The effective line width of the laser frequency at the location of the trapped atoms is deduced from the observed contrast of the interference signal for different delays T as 2 kHz. The pulses for interferometry are cut from single beams with Acousto-Optic Modulators (AOM).

The pulsed scheme demands a cyclic experiment. A typical cycle starts with trap loading for about 10 ms. To avoid line shifts and destruction of coherence, the trapping light and the quadrupole magnetic field are switched off within 20 μs before the interferometry pulses irradiate the freely expanding atomic cloud. The total trap-off time is 300 μs and the delay T between copropagating pulses is chosen here between 6.3 and 12.5 μs. After the four-pulse sequence, the trap is switched on

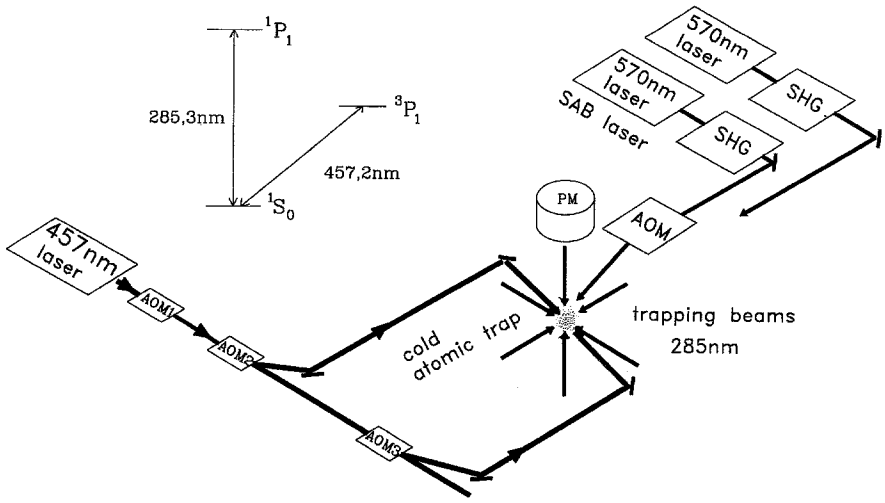

Fig. 3. Sketch of the experimental setup for interferometry with trapped Mg atoms in the presence of a pulsed light-shift potential. The *inset* shows the energy levels relevant for interferometry and the generation of the light-shift potential

again and its fluorescence is monitored. The decrease in the trap fluorescence is a quantum-amplified measure of the number of transitions to the longlived (5.1 ms) $^3P_1$ energy level. Typically, 1% of the trapped atoms are excited to the metastable state in a single cycle. Repeating the cycle many times during the life time of the undisturbed trap, the losses due to metastable excitation are accumulated and the number of trapped atoms tends to a new equilibrium value. With 1% excitation probability for a single cycle, a 30% decrease of the stationary fluorescence is achieved.

The laser beam for the additional light-shift potential is generated by a second frequency-doubled dye laser (SAB laser in Fig. 3). The Gaussian-beam profile of the widened beam ($w_x \times w_y = 2.9 \times 3.7\ mm^2$) guarantees a sufficiently homogeneous intensity distribution over the cloud of atoms, so that the phase shift varies less than 2% for all atoms contributing to the interference signal. The potential is pulsed by chopping the beam with an Acousto-Optic Modulator. The pulse rise time of 50 ns is sufficiently long to ensure adiabatic evolution for detuning values $\Delta_{uv} \gg 2\pi 20$ MHz.

The light-shift pulses of duration T' ranging between $2\ \mu s \leq T' \leq 4\ \mu s$ are applied during the dark time between equivalent beam-splitter pulses. Several fringes of the interference pattern are recorded by scanning the frequency of the beam-splitter pulses. To suppress the influence of the drift of the dye laser spectrometer on the determination of the phase shift, the interference signals are recorded at every frequency step with and without the additional light-shift pulses. The fluorescence signal is integrated for 2 s per frequency step. From the raw data, a signal background consisting of Doppler profile and saturation dip from the incoherent excitation is subtracted leaving typical interference signals as shown in Fig. 4.

For the data presented in Fig. 4, a delay between the beam-splitter pulses of $T = 6.3\ \mu s$ was chosen, leading to a periodicity of the Ramsey fringes of 79 kHz. This way, constructive overlap of the fringes from the two recoil components separated by 79 kHz is achieved. The center of the frequency axis is chosen midway between the recoil components. The fading fringe contrast for higher values of the frequency offset stems from the frequency dependence of the single-pulse-excitation probability leading to an envelope of the fringes with a half width about 200 kHz. The detected noise of the data is in accordance with the shot-noise fluctuations of the number of trapped atoms. Superimposed onto the data is a fitted model function (solid lines in Fig. 4). The phase shift between the two interference signals (upper curve recorded with and lower curve recorded without the additional potential) of 2.9 rad in the shown example is extracted from the fit data. From typical data sets, the phase shift can be deduced within an error of 0.1 rad. Besides the statistical error, a drift of the light-shift-beam intensity during the recording of a scan leads to an additional systematic uncertainty of the same magnitude.

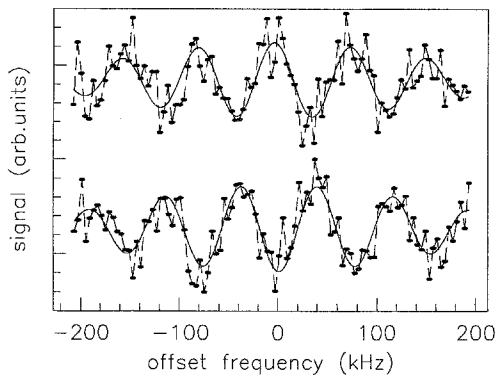

Fig. 4. Interference signals obtained on trapped Mg atoms with (*upper curve*) and without (*lower curve*) the additional light-shift potential. Successive data points (*filled circles*) are connected by *broken lines*. The *solid line* is a fit to the data. The parameters of the light-shift pulse are: $T' = 2.5\ \mu s$, $P = 15\ mW$, $\Delta_{uv} = 0.6\ GHz$

The fringe contrast of the phase-shifted interference signal is slightly reduced compared to the undisturbed interference signal. This reduction is caused by small fluctuations in the light-shift-beam intensity during the recording of a single data point. The mean value of the phase shift is unaffected since the fluctuations are effectively averaged by integrating the fluorescence signal over many interferometer cycles, but the contrast of the integrated signal is reduced.

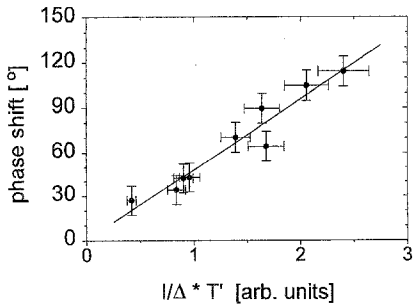

Fig. 5. Observed phase shifts from a series of scans for different parameters of the light-shift pulse. The *solid line* is a straight-line fit to the data. Error bars in x-direction contain the uncertainty of the intensity measurement. The systematic calibration error for the intensity is suppressed by using arbitrary-scaled axis

To check the dependence of the phase shift on the parameters of the potential, the phase shift was measured for several values of the light-shift-laser intensity I, detuning Δ_{uv}, ranging from 0.2 to 2 GHz, light-shift-pulse duration T', and for different values of the delay T between the beam-splitter pulses. For all measured sets of parameter values, the additional phase was found to depend only on the expected combination (Fig. 5):

$$\Phi_{\text{add}} \propto \frac{I}{\Delta} T'. \tag{7}$$

By variation of the delay T between the beam-splitter pulses, the path in space-time of the interfering particles was varied. The phase shift was found to be independent of the delay between the beam-splitter pulses. As outlined in the previous section, this observation clearly indicates the topological character of the phase shift.

The magnitude of the phase shift can be calculated using (6) if the absolute value of the UV intensity I experienced by the interfering atoms is known. This requires a careful calibration of the intensity at the position the trap. The accuracy of our measurement of UV power and beam profile allows to determine the intensity outside the vacuum can to within 20%. For the data presented in Fig. 4, where special care was taken to optimize the quality of the beam profile and the alignment to the tiny spot of trapped atoms, measured and calculated phase shift (2.9 vs 3.5 rad) agree within this uncertainty. The data presented in Fig. 5 were obtained in a separate run, with only a relative determination of the intensity values. For this reason, the proportionality constant in (7) and Fig. 5 has not been assigned at present. With a more accurate calibration of the UV intensity measurement, a similar experiment will allow the determination of an improved value for the $^1S_0$–$^1P_1$ transition dipole moment.

4 Conclusion

The light-shift potential resulting from the interaction of an optical field with the induced atomic dipole was used to measure a topological phase shift in a cold-atom interferometer. This represents the experimental verification of the extension of Aharonov and Bohm's original idea—electrons interfering in the presence of pulsed electrostatic fields — to higher multipoles. One advantage of cold-atom interferometry results from the low velocities involved, so that interference takes place in a small volume of space. This facilitates creating spatially constant interaction potentials, a fact that is very important when trying to avoid the appearance of classical forces, as gradients of these potentials.

Light-shift potentials are simple to realize, and, in addition, allow great experimental freedom of parameters, e.g., using acousto-optic and electro-optic modulators for intensity, phase and polarization control. This opens up the possibility of interesting extension of this experiment. For instance, a controlled phase modulation of the light-shift pulse creates a non-trivial path of the ground state on the Bloch sphere. This way, a resulting geometrical phase can be observed [38].

References

1. O. Carnal, J. Mlynek: Phys. Rev. Lett. **66**, 2689 (1991)
2. D.W. Keith, C.R. Ekstrom, Q.A. Turchette, D.E. Pritchard: Phys. Rev. Lett. **66**, 2693 (1991)
3. F. Riehle, Th. Kisters, A. Witte, J. Helmcke, Chr. J. Bordé: Phys. Rev. Lett. **67**, 177 (1991)
4. M. Kasevich, S. Chu: Phys. Rev. Lett. **67**, 181 (1991)
5. F. Shimizu, K. Shimizu, H. Takuma: Phys. Rev. A **46**, 17 (1992)
6. Ch. Miniatura, J. Robert, O. Gorceix, S. LeBoiteux, V. Lorent, J. Reinhardt, J. Baudon: Phys. Rev. Lett. **69**, 261 (1992)
7. M. Kasevich, S. Chu: Appl. Phys. B **54**, 321 (1992)
8. J. Robert, Ch. Miniatura, O. Gorceix, V. Lorent, S. LeBoiteux, J. Reinhardt, J. Baudon: J. Phys. II (Paris) **2**, 601 (1992)
9. U. Sterr, K. Sengstock, J.H. Müller, D. Bettermann, W. Ertmer: Appl. Phys. B **54**, 341 (1992)
10. V. Rieger, K. Sengstock, U. Sterr, J.H. Müller, W. Ertmer, Opt. Commun. **99**, 172 (1993)
11. D.E. Pritchard, C.R. Ekstrom, J. Schmiedmayer, M.S. Chapman, T.D. Hammond: In *Laser Spectroscopy XI* (AIP, New York 1993) pp. 61–66
12. D.S. Weiss, B.C. Young, S. Chu: Phys. Rev. Lett. **70**, 2706 (1993)
13. G. Möllenstedt, H. Düker: Z. Phys. **145**, 377 (1956)
14. H. Rauch, W. Treimer, U. Bonse: Phys. Lett. A **47**, 369 (1974)
15. H. Maier-Leibnitz, T. Springer: Z. Phys. **167**, 386 (1962)
16. M.O. Scully, B.-G. Englert, H. Walther: Nature **351**, 111 (1991)
17. S. Haroche, M. Brune, J.M. Raimond: Appl. Phys. B **54**, 355 (1992)
18. K. Sengstock, U. Sterr, G. Hennig, D. Bettermann, J.H. Müller, W. Ertmer: Opt. Commun. **103**, 73 (1993)
19. R. Beach, B. Brody, S.R. Hartmann: Phys. Rev. A **25**, 2658 (1982)
20. Ch. J. Bordé: Phys. Lett. A **140**, 10 (1989)
21. Ch. J. Bordé, Ch, Salomon, S. Avrillier, A. van Leberghe, C. Bréant, D. Bassi, G. Scoles: Phys. Rev. A **30**, 1836 (1984)
22. Note: In contrast to the more familiar case of stationary Ramsey-Bordé interferometry with an atomic beam, scanning the detuning here leads to non-dispersive phase shift
23. Th. Kisters, K. Zeiske, F. Riehle, J. Helmcke: Appl. Phys. B **59**, 89 (1994)
24. K. Sengstock, U. Sterr, J.J. Müller, V. Rieger, D. Betterman, W. Ertmer: Appl. Phys. B **59**, 99 (1994)
25. Y. Aharonov, D. Bohm: Phys. Rev. **115**, 485 (1959)
26. J. Anandan: Phys. Lett. A **138**, 347 (1989)
27. S. Olariu, I.I. Popescu: Rev. Mod. Phys. **57**, 339 (1985)
28. R.G. Chambers: Phys. Rev. Lett. **5**, 3 (1960)
29. J. Anandan: Phys. Rev. Lett. **48**, 1660 (1982)
30. Y. Aharonov, A. Casher: Phys. Rev. Lett. **53**, 319 (1984)
31. A. Cimmino, G.I. Opat, A.G. Klein, H. Kaiser, S. Werner, M. Arif, R. Clothier: Phys. Rev. Lett. **63**, 3803 (1989)

32. K. Sangster, E.A, Hinds, S.M. Barnett, E. Riis: Phys. Rev. Lett. **71**, 3641 (1993)
33. M. Wilkens: Phys. Rev. Lett **72**, 5 (1994)
34. A. Zeilinger: In *Fundamental Aspects of Quantum Theory*, ed. by V. Gorini, A. Frigerio (Plenum, New York 1985) pp. 311–318
35. B.E. Allman, A. Cimmino, A.G. Klein, G.I. Opat, H. Kaiser, S.A. Werner: Phys. Rev. Lett. **68**, 2409 (1992)
36. G. Badurek, H. Weinfurter, R. Gähler, A. Kollmar, S. Wehinger, A. Zeilinger: Phys. Rev. Lett. **71**, 307 (1993)
37. S. Nic Chormaic, Ch. Miniatura, O. Gorceix, B. Viaris de Lesegno, J. Robert, S. Feron, V. Lorent, J. Reinhardt, J. Baudon, K. Rubin: Phys. Rev. Lett. **72**, 1 (1994)
38. M. Reich, U. Sterr, W. Ertmer: Phys. Rev. A **47**, 2518 (1993)